JOURNAL OF MATERIALS SCIENCE: MATERIALS IN MEDICINE 9 (1998) 701–706

In vivo skeletal response and biomechanical assessment of two novel polyalkenoate cements following femoral implantation in the female New Zealand White rabbit

M. C. BLADES, D. P. MOORE, P. A. REVELL*
Royal Free Hospital School of Medicine, Department of Histopathology and Comparative Biology Unit, Rowland Hill Street, London NW3 2PF UK

R. HILL
Department of Materials Science, University of Limerick Limerick Ireland

Glass-ionomer cements (GIC) offer several advantages over the conventional acrylic-based bone cements. The formation of an adhesive bond with bone and metals, a low setting exotherm and no systemic or local toxicity are some of the advantages cited. This study examines the *in vivo* biological and biomechanical behavior of two polyalkenoate cements (LG26 and LG30) implanted for 6 wk into the submetaphyseal spongiosa of the rabbit femur. Cements were implanted as both set cement rods and unset cement dough. Implantation of set rods resulted in the formation of variably mineralized osteoid/woven bone at the bone–cement interface. Mechanical (push-out) testing revealed the strength of this bone–cement interface was of similar magnitude to control (PMMA-rod implanted) animals. The bone of LG cement-dough implanted animals exhibited demineralization of pre-existing bone local to the site of implantation, accumulation of aluminum both locally and at a distance from the site of implantation, and defective mineralization of newly formed osteoid. The histological picture following LG implantation was strikingly similar to human renal osteodystrophy, in which skeletal accumulation of aluminum is a noted feature. The development of a GIC with low/no aluminum release from the unset cement dough is a priority in the further development of these cements for possible orthopaedic applications.

1. Introduction

Conventional polymethylmethacrylate (PMMA) bone cements have been used extensively in clinical practice for over 30 y. During this time, a range of problems associated with their physical and chemical properties have been identified. The systemic toxicity of methylmethacrylate monomer has been implicated in acute cardiovascular and respiratory reactions observed during cemented arthroplasty [1], though the pathological mechanisms of such reactions remain in debate [2, 3]. Thermal damage to the cortex during the *in situ* exothermic curing of the cement may lead to local osteonecrosis, thus compromising the bone healing response at the site of implantation [4]. Also, PMMA cements rely on mechanical interlocking with bone and implant rather than adhesive chemical bond formation to form a stable bone–implant union.

Glass polyalkenoate (glass-ionomer, GIC) cements are formed by the combination of concentrated polymeric acid (polyacrylic acid) with an acid degradable fluoro-alumino-silicate glass. The setting reaction relies on the glassy phase to contribute cations to cross-link the polymer chains. As the setting reaction is one of neutralization (salification) rather than polymerization, there is, in contrast to PMMA-based cements, little or no exotherm associated with the reaction. Additionally, GIC's have been shown to form adhesive bonds between bone and metals [5]. Their potential for bioactivity is illustrated by their ability to release osteoconductive ions such as calcium and fluoride for prolonged periods post-setting [6], an attractive characteristic for a surgical bone cement.

This study examines the *in vivo* biological and biomechanical behavior of two candidate glass-ionomer cements, LG26 and LG30, implanted as set cement rods and cement dough and compares the tissue reaction to that seen following the implantation of conventional (PMMA) orthopaedic cement.

*Author to whom all correspondence should be addressed.

2. Materials and methods

2.1. Implant materials

Two experimental glass-ionomer cements were used (LG26 and LG30, Department of Materials Science, University of Limerick, Ireland). Conventional polymethylmethacrylate-based orthopaedic cement (Surgical Simplex) was employed as a control implant material. The glass-based cements had a Ca : P ratio of 1.66 and the following general chemical formula $(P)SiO_2(Q)Al_2O_3(5\text{-}X)CaO \cdot 1.5P_2O_5(X)CaF_2$, where P, Q and X are the mole fractions. During production of glasses with higher CaO content, the mole fractions of alumina and silica were increased to ensure glass formation. As the fluoride content of the glass was varied by the addition of CaF_2, the CaO content was modified by the variable X, where for LG26 $X = 2$ and for LG30 $X = 0$.

2.2. Formation of cylindrical implants

Glass-ionomer cements were produced using a ratio of 1 g glass, 0.2 g freeze-dried mercaptan free poly-acrylic acid (Advanced Healthcare, UK), 0.3 ml Sterile non-pyrogenic water. Prior to use, all implant materials were sterilized by gamma irradiation (3.5 MRad; Swann Morton Ltd, UK). Implant rods (length 10 mm, diameter 3.5 mm) were produced 24 h prior to implantation by placing unset material in PTFE molds. Implants were cured for 5 h at room temperature. The implants were then sterilized by UV irradiation (254 mm) overnight at room temperature in sealed, humidified containers. PMMA cement was prepared according to the manufacturer's instructions, with implants cast and sterilized in an identical manner to the above.

For implantation of cement dough, pre-weighed sterile components were mixed aseptically immediately prior to implantation on refrigerated, sterile glass or perspex mixing slabs. Care was taken to ensure the through incorporation of all dry components into the mixed cement and that the mixed cement was of uniform consistency between animals.

2.3. Implantation and histological examination

Female New Zealand White rabbits (2.5–3.5 kg body weight) were used throughout. Under general anaesthesia (Hypnorm/Diazepam induction; Halothane 2% (May and Baker, UK) in oxygen 25%, nitrous oxide 50% maintenance), cylindrical defects of the same diameter as the implant cylinders were created in the distal femoral intercondylar notch of rabbits using a saline-cooled 3.5 mm diameter orthopaedic drill (AO, Switzerland). Defects were filled with sterile cement dough (PMMA, LG26 or LG30; $n = 6$ per implant material), or sterile pre-set cement rods ($n = 12$ per implant material). Fluorochrome bone labels were administered by subcutaneous injection at intervals of 7 d in those animals to be used for histological assessment (Table I). Animals to be used for mechanical testing received no bone labels.

TABLE I Fluorochrome administration schedule

Fluorochrome administered	Day of administration (Day 0 = date of surgery)
Tetracycline	7
Calcein green	14
Alizarin complexone	21
Calcein blue	28
Calcein green	35

All animals were sacrificed 42 d postoperatively by intravenous barbiturate overdose (Sagital, Bayer, UK). The implanted femur from six animals in each treatment group was processed for histological examination using the Exakt technique [7]. Sections for histological analysis were stained with toluidine blue. The tissue distribution of fluorochrome labels was assessed in unstained sections by UV-microscopy. Tissue mineralization in the interface and surrounding trabecular bone was assessed histochemically using the von Kossa technique and by scanning electron microscopy (SEM) EDAX analysis. Cement-derived aluminum distribution was determined histochemically using the aluminon method [8] and confirmed by SEM EDAX analysis.

2.4. Mechanical testing

All mechanical testing was performed using an Instron 4464 test machine fitted with a 2 kN load cell. The mechanical strength of the bone–cement interface, in set-rod implanted animals, was determined by measurement of the interfacial shear strength (ISS) using push-out testing [9]. Sections 8 mm thick of frozen implanted femur were prepared using an Exakt diamond band saw, such that the cut surfaces of the specimens lay perpendicular to the implant surface. Prior to push-out testing, specimens were thawed in Ringers solution at 37 °C. A specially prepared testing jig was used (for details see [9]) to ensure that the applied force was perpendicular to the cut surface of the implant. A crosshead velocity of 1 mm min^{-1} was employed and Ringers solution at 37 °C was pipetted on to the specimens during testing to maintain a hydrated environment. Post-mortem set-rod implanted femora were tested in an identical manner to assess the frictional contribution to the measured ISS.

3. Results

3.1. Biocompatibility

By 6 wks, bone had grown to surround both the PMMA and LG set-rod implants. In all cases, the PMMA control implants were surrounded by trabecular bone which was circumferentially arranged but separated from the implant by a partial fibrous tissue membrane. Bone had remodeled in a similar way around the LG26 and LG30 set-rod implants. This, however, was separated from the underlying trabeculae by woven bone or osteoid formation (Fig. 1a, b). Examination of mineralization by the von Kossa technique revealed well-mineralized trabecular

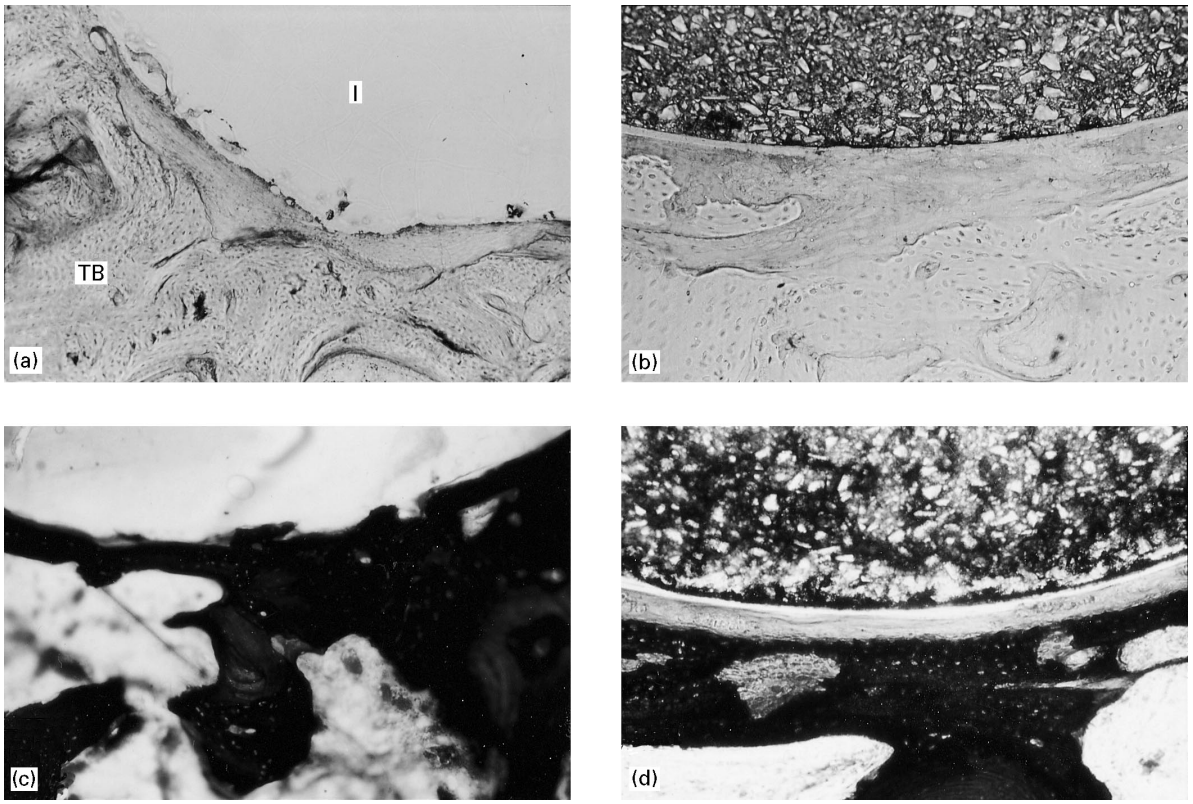

Figure 1 Histological reaction to set cement rod implantation. (a) PMMA. Thickened, cellular, fibrous layer present between underlying trabecular bone (TB) and implant (I). Toluidine blue stain, ×100. (b) LG26. Osteoid/woven bone formation at the bone : cement interface. Toluidine blue stain, ×100. (c) PMMA. Mineralized (black staining reaction) bone at the bone : cement interface. von Kossa stain, ×100. (d) LG26. Unmineralized osteoid/fibrous tissue at the bone : cement interface. von Kossa stain, ×100.

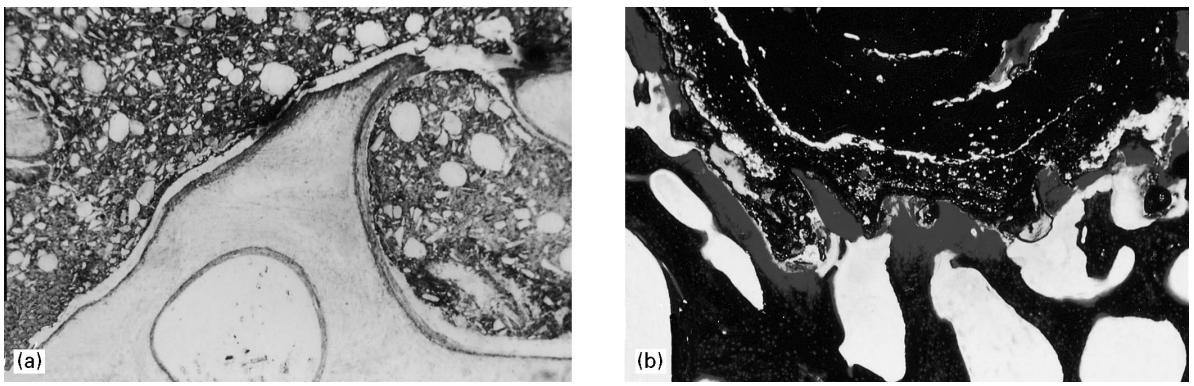

Figure 2 Histological reaction to cement-dough implantation: (a) LG26. Thickened osteoid seams are present at the interface between cement and bone. Toludine blue stain, ×100. (b) LG26. Demineralized trabecular bone (red staining reaction) is shown at the cement : bone interface. Von Kossa stain, ×30.

bone in apposition to the PMMA implants. By contrast, the interfacial tissues in LG26 and LG30 implanted animals were partially mineralized (Fig. 1c, d). Trabecular bone distant from the implant site was of normal appearance.

In cement-dough implanted animals, the histological reaction and degree of mineralization following PMMA implantation was similar to that seen after PMMA set-rod implantation. Following LG26 and LG30 cement-dough implantation, a mixture of poorly mineralized osteoid and fibrous tissue reaction was observed in apposition to the implant surface. Additionally, pre-existing trabecular bone in the vicinity of the implants was observed to be extensively demineralized when stained using the von Kossa technique. In places, demineralized trabecular spurs close to the implant surfaces were observed in continuity with well-mineralized trabecular not apposed to the implant (Fig. 2a, b). Additionally, trabecular bone distant to the site of implantation was extensively covered by prominent osteoid seams.

Examination of unstained undecalcified sections of set-rod implants by UV-fluorescence microscopy revealed patterns of mineralization in osteoid seams surrounding the implant materials. These comprised both calcification in a woven bone pattern and linear deposition of calcium by appositional bone formation (trabecular remodeling). PMMA-implanted tissues

exhibited appositional bone formation in the implant vicinity with continuing bone formation throughout the post-operative period (Fig. 3a, b). By contrast, in LG26 and LG30 implanted animals, patchy tetracycline fluorescence was observed corresponding to the mineralization of woven bone in the implant vicinity at day 7. Trabecular bone distant to the implant site in all set-rod implanted animals showed normal patterns and amount of mineralization.

UV-fluorescence microscopy of PMMA cement-dough implanted animals revealed similar patterns of label uptake to those seen in the set-rod implanted control animals. In LG26 and LG30 implanted animals there was no evidence of fluorochrome uptake in the vicinity of the implant materials. Additionally, fluorochrome uptake was absent from bone surrounding the site of implantation.

3.2. Tissue distribution of cement-derived aluminum

No evidence of aluminum incorporation was seen in either control groups on sections stained by the aluminon technique (Fig. 4a). In LG26 and LG30

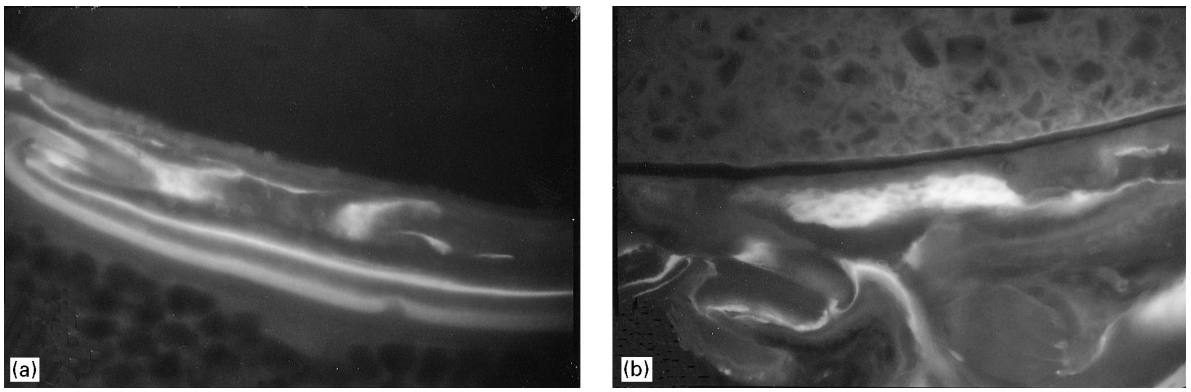

Figure 3 UV-microscopy of fluorochrome incorporation following set-rod implantation. (a) PMMA. Lamellar mineralization of osteoid adjacent to the implant. Flourescent bands corresponding to tetracycline (yellow), calcein green (pale green) and alizarin complexone (red) are present; × 100. (b) LG26. Patchy mineralization of woven bone at the cement–bone interface is demonstrated by tetracycline incorporation (yellow). Tetracycline and calcein green incorporation into osteoid seams in the surrounding trabecular bone is also shown; × 100.

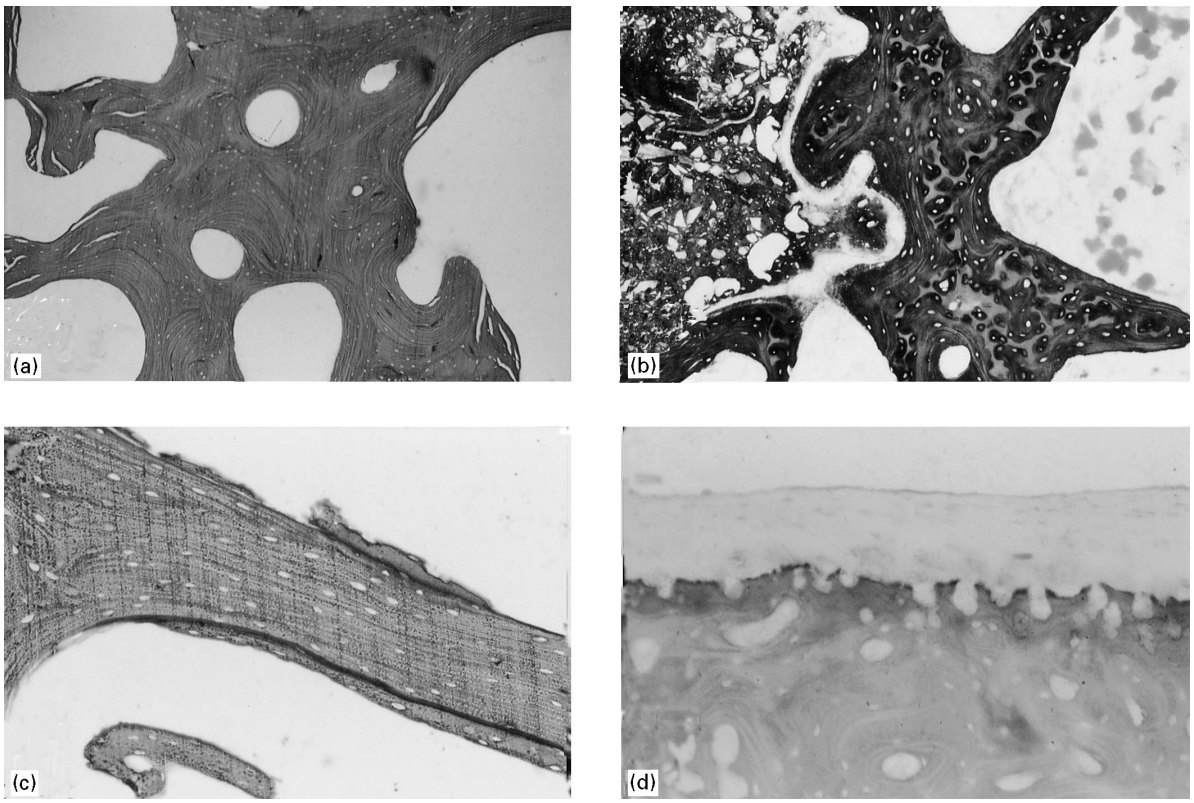

Figure 4 Histochemical detection of aluminum by the aluminon technique. (a) PMMA dough-implanted femur. No aluminum deposition was demonstrable in the trabecular bone or osteoid of PMMA implanted (control) animals. Aluminon/methylene blue, × 100. (b) LG26 dough-implanted femur. Aluminum (dark red staining reaction) is present throughout the trabecular bone adjacent to the implant site. Aluminon/methylene blue, × 100. (c) LG26 dough implanted femur. Aluminum positive cement lines in trabecular bone distant to the implant site. Aluminon/methylene blue, × 200. (d) LG26 dough-implanted femur. Aluminum deposition is seen at the junction (tide mark) between femoral articular cartilage and underlying cortical bone. Aluminon/methylene blue, × 100.

set-rod implanted femora, aluminum was localized to the implant surface and interfacial tissues. However, in LG26 and LG30 cement-dough implanted animals, marked deposition of aluminum was observed in bone adjacent to, and distant from the implant surface. Interfacial osteoid/bone was heavily stained for aluminum (Fig. 4b). Trabecular osteoid and cement lines were also positively stained distant to the site of implantation (Fig. 4c). Additionally, aluminum was demonstrable at the tide mark between articular cartilage and mineralized cortical bone (Fig. 4d).

EDAX analysis was performed on ground sections of LG26 and LG30 dough-implanted femora. Spot analyses of trabeculae revealed both silicon and aluminum accumulation both in the vicinity of the implant and in the surrounding trabecular bone (Fig. 5a). Aluminum and silicon were also demonstrable at articular cartilage–bone interface (Fig. 5b). No aluminum or silicon was demonstrable in PMMA-implanted bone.

3.3. Mechanical testing

Measurements of interfacial shear stress carried out on post-mortem implanted femora indicated a frictional contribution of less than 0.1 MPa to the total interfacial shear stress. No significant difference in maximum interfacial shear stress was noted either between PMMA (0.21 ± 0.12 MPa (mean $\pm$ S.D.)) LG26 (0.38 ± 0.25 MPa) or LG30 (0.35 ± 0.14 MPa) implanted material (Fig. 5).

4. Discussion

The histological response to GIC-cement dough implantation was similar in severity and presentation regardless of cement composition or formulation. In GIC-dough implanted femora, the interface consisted of pre-existing trabecular bone interspersed with poorly organized osteoid/woven bone. Examination of bone mineral distribution by the von Kossa technique revealed variable demineralization of pre-existing trabecular bone at the implant site. UV-microscopy revealed no fluorochrome label incorporation into the interfacial tissues. In addition, osteoid mineralization distant to the site of implantation was markedly inhibited. These results are consistent with those of Erbe *et al.* [10] using a GIC (IONOCEM) to cement a hemiarthroplasty into the rabbit femur. They describe a disturbance of mineralization, osteoid formation at the interface, and poor mechanical properties of the cement in this load-bearing environment.

PMMA-implanted femora showed no evidence of aluminum incorporation using the aluminon technique. In contrast, GIC dough-implanted femora showed marked distribution of GIC-derived aluminum into bone adjacent to and distant from the implant surface. Additionally, aluminum was identified at the articular cartilage/bone interface, in synovial macrophages, and in bone marrow inflammatory infiltrates.

GIC-dough implantation studies revealed bone demineralization local to the site of implantation. It was

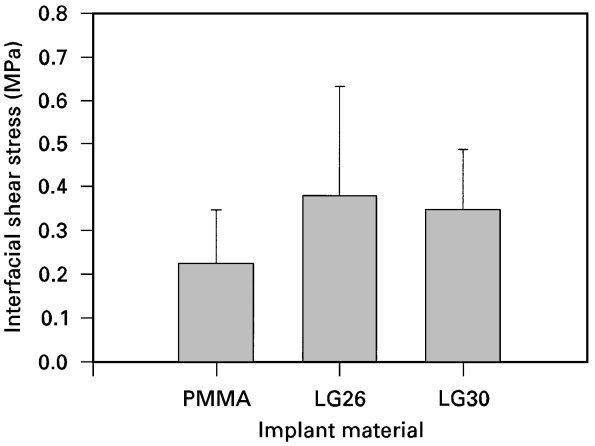

Figure 5 Mechanical (push-out) test results. Bars represent group means; error bars $\pm$1S.D. ($n = 5$).

thought likely that this resulted from the generation of a low pH environment at the site of implantation following the introduction of acidic unset GIC material. Such an environment would favor the dissolution of bone mineral. This hypothesis was supported by the findings of no local demineralization following the implantation of GIC set cement rods.

GIC-derived aluminum was widely distributed in femora following cement implantation. Aluminum was demonstrable by histochemistry (aluminon method) and SEM EDAX analysis. The site-specific accumulation of aluminum was similar to that demonstrated in the bones of renal dialysis patients exposed to aluminum in dialysates or aluminum containing phosphate binding agents [11–13]. Although aluminum intoxication is not a pre-requisite of osteodystrophy in patients with renal insufficiency, aluminum intoxicated individuals typically show higher morbidity and poorer response to clinical intervention than non-intoxicated individuals [14].

Experimental animal studies have demonstrated aluminum deposition in trabecular osteoid and cement lines associated with osteomalacia-like lesions [15, 16]. Electron microprobe techniques have shown aluminum to be accumulated as the hydroxide in the lysosomes of several mammalian cell types following parenteral administration [17, 18]. Additionally, periosteally derived bovine osteoblasts and osteoclasts were shown to accumulate and store GIC-derived aluminum in an *in vitro* biocompatibility study [19]. An insight into the possible mechanisms of aluminum deposition and osteo-toxicity was given by Talwar *et al.* [20]. *In vivo* mineralization of subcutaneously implanted demineralized bone matrix was inhibited by parenteral aluminum salt administration. In addition, aluminum salts implanted locally with the matrix appeared to be toxic to cells associated with osteogenesis and chondrogenesis.

Clearly, in the interests of biocompatibility, aluminum release from GIC-cements intended for orthopaedic applications should be minimized. The inhibition of osteoid seam mineralization, both locally and at a distance from the site of GIC dough-implantation, together with the abundance of aluminum containing osteoid seams and cement lines, shows

a pattern of pathology strikingly similar to that of human renal osteodystrophy. As aluminum release from the cements was minimal in set-rod implanted animals, further work should seek to minimize levels of labile aluminum during the setting reaction.

5. Conclusions

GIC dough-implantation in the rabbit femora leads to two distinct pathological lesions. Demineralization of local trabecular bone occurs in the short-term, following implantation. Aluminum, released from the setting cement, accumulates in regions of bone formation, both locally and at a distance from the implant material, inhibiting mineralization of osteoid and possible remineralization of previously demineralized bone. The histological picture presented is similar to that described in human renal osteodystrophy.

In order for the Limerick glass formulations to be credible as surgical bone cements, the development of a low-aluminum releasing formulation is a priority. In such a formulation, the relative merits conferred by the incorporation into the glass of bioactive ions, such as fluoride, may be examined without the confounding influence of toxic levels of aluminum.

Acknowledgment

This work was funded by Brite EurAm project no: BRE2.CT92.0349.

References

1. R. F. CONVERY, D. R. GUNN, J. D. HUGHES and W. E. MARTIN, *J. Bone Joint Surg.* **57** (Am) (1975) 57.
2. M. TRYBA, I. LINDE, G. VOSHAGE and M. ZENZ, *Anaesthatist* **40** (1991) 25.
3. J. F. M. RUDIGIER and G. RITTER, *Res. Exp. Med.* **183** (1983) 77–94.
4. B. MJÖBERG, H. PETTERSSON, R. ROSENQVIST and A. RYDHOLM, *Acta Orthop. Scand.* **55** (1984) 597.
5. D. WOOD and R. HILL, *Biomaterials* **12** (1991) 164.
6. P. V. HATTON and I. M. BROOK, *Br. Dent. J.* **173** (1992) 275.
7. M. D. ROHRER and C. C. SCHUBERT, *Oral Surg. Oral Med. Oral Pathol.* **74** (1992) 73.
8. N. A. MALONEY, S. M. OTT, A. C. ALFREY, N. L. MILLER, J. W. COBURN and D. J. SHERRARD. *J. Lab. Clin. Med.* **99** (1982) 206.
9. K. A. HING, S. M. BEST, K. E. TANNER, W. BONFIELD and P. A. REVELL, *J. Mater. Sci. Mater Med.* **8** (1997) 731.
10. M. ERBE, R. L. VAN DYKE-ERBE and H. J. SCHMITZ, *ibid.* **7** (1996) 517.
11. S. M. OTT, N. A. MALONEY, J. W. COBURN, A. C. ALFREY and D. J. SHERARD, *N. Engl. J. Med.* **307** (1982) 709.
12. S. P. ANDREOLI, M. J. BERGSTEIN and D. J. SHERRARD, *ibid.* **310** (1984) 1079.
13. N. A. MALONEY, S. M. OTT, C. A. ALFREY, N. L. MILLER, J. W. COBURN and D. J. SHERRARD, *J. Lab. Clin. Med.* **99** (1982) 206.
14. D. J. SHERRARD, G. HERCZ, Y. PEI and G. SEGRE, *Nephrol. Dial. Transpl.* **11** (1996) 29.
15. G. JABLONSKI, K. H. KLEM, C. C. DANIELSEN, L. MOSEKILDE and J. O. GORDELADZE, *Biosci. Rep.* **16** (1996) 49.
16. W. G. GOODMAN, J. GILLIGAN and R. HORST, *J. Clin. Invest.* **73** (1984) 171.
17. J. P. BERRY, *Cell. Molec. Biol.* **42** (1996) 395.
18. M. FIEJKA, E. FIEJKA and M. DLUGASZEK, *Pharmacol. Toxicol.* **78** (1996) 123.
19. U. MEYER, D. H. SZULCZEWSKI, K. MOLLER, D. B. JONES and P. WUISMAN, *Z. Orthop. Grenzegebiete* **134** (1996) 117.
20. H. TALWAR, H. REDDI, J. MENCZEL, W. THOMAS and L. MEYER, *Kidney Int.* **29** (1986) 1038.

Received 7 May
and accepted 27 May 1998